Acta Cybernetica **27** (2026) 337–357.

Ultra-Wideband Smart Wheelchair Pose Estimation Using Interval Analysis

Théo Le Terrier[ab], Marie Babel[ac], and Vincent Drevelle[ad]

Abstract

In this paper, we introduce a reliable positioning method for a smart wheelchair by using ultra-wideband (UWB) technology. This method provides confidence domains of the pose by assuming bounded measurement errors and proprioceptive information, without any assumptions of independence. Exploiting interval analysis and constraint propagation techniques, we characterize the sets of all feasible poses that are consistent with the measurements. Our method has been validated through experiments with a smart power wheelchair equipped with UWB sensors in realistic conditions. The results demonstrate that our approach consistently provides guaranteed uncertainty domains with 100% integrity across the tested dataset, even when faced with inconsistent measurements. In addition, we compare our interval-based method with M-estimator approaches, and show that while achieving slightly worse positioning accuracy, our method offers superior consistency.

Keywords: localization, interval analysis, ultra-wideband, smart wheelchair

1 Introduction

Preserving independence and access to social activities is essential for wheelchair users. Indeed, a decrease in mobility can lead to reduced self-esteem, isolation and fear of abandonment [9]. However, operating power wheelchairs requires significant driving skills, which might prove infeasible for people with cognitive impairments or visual deficiencies. To make this assistive technology more accessible, *smart wheelchairs* have been proposed by enhancing standard power wheelchairs with sensors and embedded systems. These advanced robotic assistive devices aim to provide safe navigation assistance, thereby preserving the user's independence and social engagement. Both autonomous [27, 24] and semi-autonomous [25, 7] navigation systems have emerged to provide the right level of assistance to the user.

[a]Univ Rennes, INSA Rennes, Inria, CNRS, IRISA – UMR 6074, F-35000 Rennes, France
[b]E-mail: theo.le-terrier@irisa.fr, ORCID: 0009-0000-8800-7159
[c]E-mail: marie.babel@irisa.fr, ORCID: 0000-0001-6425-389X
[d]E-mail: vincent.drevelle@irisa.fr, ORCID: 0000-0001-9579-7793

DOI: 10.14232/actacyb.315261

Fully autonomous navigation systems face the challenge of localization, which can be addressed with integrated smart wheelchair sensors. For widespread adoption, the localization system should offer low cost, easy attachment to any smart wheelchair, robustness and efficiency [20]. Also, for privacy concerns and acceptability reasons, visual sensors are avoided.

This paper proposes a reliable positioning method for a smart wheelchair, using a set of ultra-wideband (UWB) sensors [3]. The latter have gained popularity for indoor robotics where GNSS signals are unavailable, and commercially available sensors such as the DWM1001 by Qorvo meet the aforementioned requirements. A typical UWB-based positioning setup involves fixed UWB nodes (*anchors*), measuring their distance from UWB nodes on the robot (*tags*). Statistical approaches have been commonly considered to design UWB based positioning systems: nonlinear least squares [2, 17], or Kalman filters [21, 22]. In these papers, UWB measurement error distributions are modeled as Gaussian, and independence between each measurement from one time to another is assumed. Such assumptions are reasonable when considering line-of-sight (LOS) signal propagation. The case of non-line-of-sight (NLOS) signal propagation in multipath environments was also widely explored in the field of probabilistic methods [5, 16], with e.g., particle filters [11]. Furthermore, with access to the UWB channel estimation data and additional prior knowledge on the initial receiver position and moving direction, the localization process can be based on the estimated multipath components [10].

An alternative to make as less assumptions as possible is to assume only a *bounded-error model*, meaning that measurement errors and model parameters are within known bounds. Set-membership estimators then compute a domain of solutions consistent with the model and the measurements without removing any feasible solution. Interval analysis [14] provides tools to compute such domains and has been used for reliable pose estimation [23, 26] in various contexts, including aerial robotics [18], marine applications [28], and underwater robotics [13, 29]. These systems typically use sensors like cameras or sonars. GNSS receivers have also been employed for reliable positioning of outdoor vehicles [8, 30], sometimes in combination with UWB [1]. However, to our knowledge, interval methods have not been applied to indoor UWB localization.

The main contribution of this paper is a reliable UWB based positioning method using interval analysis and an experimental validation of the latter in a realistic scenario, involving a user in a smart wheelchair. Our approach is compared with M-estimator methods (classical Huber [12], and the half-Cauchy of [16]).

This paper is structured as follows. We first provide an overview of the pose estimation problem and introduce interval analysis and robust set inversion. We then present our proposed method and conclude with experimental results using UWB sensors mounted on a smart wheelchair.

2 Problem Statement

In this paper, we aim to provide a reliable 2-D pose estimation of a smart wheelchair equipped with UWB sensors. The wheelchair is operated by a user-controlled joystick. The wheelchair is assumed to move in a horizontal planar world without slipping. The robot configuration is denoted $\mathbf{p} = (x, y, \theta)^T$ where (x, y) are the planar coordinates, and θ is the heading angle between the frame $\mathcal{F}_w$ and the local frame attached to the wheelchair $\mathcal{F}_r$. Assuming that the wheelchair's kinematics is similar to those of a unicycle, its continuous-time model is

$$\begin{cases} \dot{x}(t) = v(t) \cdot \cos\theta(t) \\ \dot{y}(t) = v(t) \cdot \sin\theta(t) \\ \dot{\theta}(t) = \omega(t). \end{cases} \tag{1}$$

The input commands are the linear velocity, denoted v, and the angular velocity, denoted ω. These inputs are estimated by the embedded control system (*power module*) of the power wheelchair from the joystick position. A set of UWB anchors is installed in a room, and distance measurements to UWB tags installed on the wheelchair are performed. An overview of the system is presented in Figure 1.

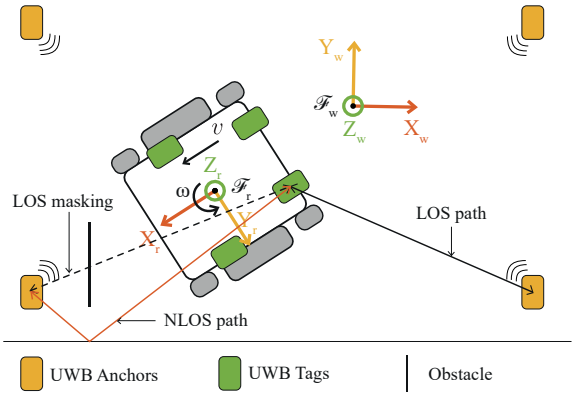

Figure 1: System Overview. Each tag (green) measures its distance to each anchor (yellow), thus estimates its own position in $\mathcal{F}_w$. The wheelchair pose is then deduced, since the positions of the tags are known in $\mathcal{F}_r$

Let n_T be the number of tags installed on the wheelchair, and n_A the number of anchors. We denote $T_{i,\, i\in\{1,\ldots,n_T\}}$, the i^{th} tag, and $A_{j,\, j\in\{1,\ldots,n_A\}}$, the j^{th} anchor. The coordinates of T_i, expressed in $\mathcal{F}_r$, are denoted ${}^r\mathbf{x}_{T_i} = ({}^rx_{T_i}, {}^ry_{T_i}, {}^rz_{T_i})$. The coordinates of T_i in $\mathcal{F}_w$ are denoted $\mathbf{x}_{T_i} = (x_{T_i}, y_{T_i}, z_{T_i})$. The fixed coordinates of A_j in $\mathcal{F}_w$, are denoted $\mathbf{x}_{A_j} = (x_{A_j}, y_{A_j}, z_{A_j})$. The measured range between T_i and A_j is denoted $r_{i,j}$ and is defined as

$$r_{i,j} = \|\mathbf{x}_{T_i} - \mathbf{x}_{A_j}\|_2 + \beta_{i,j}, \tag{2}$$

where $\beta_{i,j}$ is the range measurement error.

3 Interval Analysis and Robust Set Inversion

3.1 Interval Analysis

Interval analysis [14] relates to intervals $[x] = [\underline{x}, \overline{x}]$ and their multidimensional extension, interval vectors or boxes $[\mathbf{x}] = [\underline{\mathbf{x}}, \overline{\mathbf{x}}]$. $\underline{\mathbf{x}}$ and $\overline{\mathbf{x}}$ respectively represent the lower and upper bounds of $[\mathbf{x}]$. The *width* of an interval is defined as the difference between its upper and lower bounds. The width of a box is the width of its largest interval components. The *radius* of an interval, or box, is defined as its half-width. The set of real intervals is denoted $\mathbb{IR}$, and the set of n-dimensional boxes is $\mathbb{IR}^n$.

Let $\mathbf{f}$ be a function from $\mathbb{R}^n$ to $\mathbb{R}^m$. The image by $\mathbf{f}$ of an n-dimensional box $[\mathbf{x}]$ is a set $\mathbf{f}([\mathbf{x}])$ which is not necessarily a box (Figure 2). The *inclusion function* $[\mathbf{f}]$ from $\mathbb{IR}^n$ to $\mathbb{IR}^m$ is then defined to enclose $\mathbf{f}([\mathbf{x}])$ by a box $[\mathbf{f}]([\mathbf{x}])$ such that

$$\forall [\mathbf{x}] \in \mathbb{IR}^n, \mathbf{f}([\mathbf{x}]) \subset [\mathbf{f}]([\mathbf{x}]).$$

The smallest box containing $\mathbf{f}([\mathbf{x}])$ is returned by the minimal inclusion function $[\mathbf{f}]^*$. The smallest box enclosing a set $\mathcal{S}$ is denoted $\square\, \mathcal{S}$ and is called the *interval hull* of $\mathcal{S}$. Thus, $[\mathbf{f}]^*([\mathbf{x}]) = \square\, \mathbf{f}([\mathbf{x}])$.

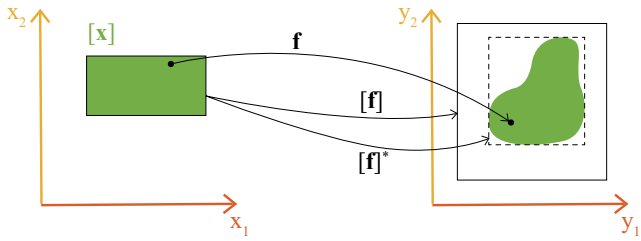

Figure 2: Image of a box $[\mathbf{x}]$ by a function $\mathbf{f}$, an inclusion function $[\mathbf{f}]$, and the minimal inclusion function $[\mathbf{f}]^\star$.

3.2 Contractors

Let $\mathbf{x}$ be a vector which variables are linked by relations, or constraints. A *Constraint Satisfaction Problem* (CSP) can be formulated $\mathcal{H} : \{\mathbf{f}(\mathbf{x}) = \mathbf{0}, \mathbf{x} \in [\mathbf{x}]\}$, where $\mathbf{f}(\mathbf{x}) = \mathbf{0}$ represents the constraints, and $[\mathbf{x}]$ the variables' domain.

Let $\mathcal{S} = \{\mathbf{x} \in [\mathbf{x}] \mid \mathbf{f}(\mathbf{x}) = \mathbf{0}\}$ be the solution set of $\mathcal{H}$. A *contractor* $\mathcal{C}$ [4] is a mapping from $\mathbb{IR}^n$ to $\mathbb{IR}^n$ such that

- $\forall [\mathbf{x}] \in \mathbb{IR}^n, \mathcal{C}([\mathbf{x}]) \subseteq [\mathbf{x}]$ (*contraction*),
- $\forall [\mathbf{x}] \in \mathbb{IR}^n, \mathcal{C}([\mathbf{x}]) \cap \mathcal{S} = [\mathbf{x}] \cap \mathcal{S}$ *(completeness).*

In other words, the variables' domain $[\mathbf{x}]$ can be reduced without excluding any solution by applying a contractor. A contractor $\mathcal{C}^\star$ is *minimal* if $\mathcal{C}^\star([\mathbf{x}])$ is the smallest box containing $\mathcal{S} \cap [\mathbf{x}]$, i.e., $\mathcal{C}^\star([\mathbf{x}]) = \square\, \mathcal{S} \cap [\mathbf{x}]$. In Figure 3 (a), $\mathcal{C}^\star$ is the minimal contractor.

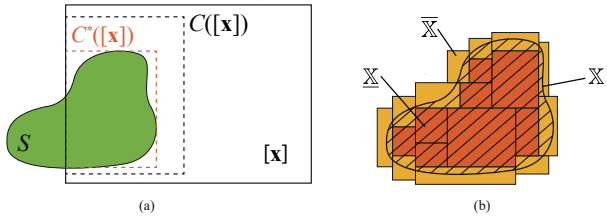

Figure 3: (a) Contractors reducing the variables' domain of a box $[\mathbf{x}]$. (b) Inner (orange) and outer (yellow) approximation of a set $\mathbb{X}$ by subpavings.

3.3 Robust Set Inversion

Let $\mathbb{Y}$ be a known subset of $\mathbb{R}^m$, e.g., obtained from m measurements. Set inversion problem [14] consists in characterizing

$$\mathbb{X} = \{\mathbf{x} \in \mathbb{R}^n | \mathbf{f}(\mathbf{x}) \in \mathbb{Y}\} = \mathbf{f}^{-1}(\mathbb{Y}).$$

Two subpavings (sets of non-overlapping boxes) that provide an *inner* and *outer* approximation of $\mathbb{X}$, i.e. such that $\underline{\mathbb{X}} \subset \mathbb{X} \subset \overline{\mathbb{X}}$, can be computed with the *Set Inversion via Interval Analysis* (SIVIA) algorithm [14]. Such subpavings are shown in Figure 3 (b). The SIVIA algorithm employs a branch and bound strategy. Starting from an initial domain $[\mathbf{x_0}]$ to which $\overline{\mathbb{X}}$ is guaranteed to belong, SIVIA performs successive contractions and bisections to refine the inner and outer approximations of the solution set. Algorithm 1 describes our *anytime* implementation, with a breadth-first exploration strategy that can be stopped after a *timeout*.

Algorithm 1 Anytime SIVIA(in: $[\mathbf{x_0}]$, $\mathcal{C}$, ϵ, *timeout* ; out: $\overline{X}$)

```
1:  X̄ ← ∅                                          Outer subpaving of the solution set
2:  L ← ([x0])                                     Add initial domain to the FIFO queue
3:  while L ≠ ∅ and time() ≤ timeout do
4:     ([x], L) ← L                                Dequeue a box from the FIFO
5:     [xc] ← C([x])                               Contract the box
6:     if [xc] ≠ ∅ then
7:        if width([xc]) > ε then                  Bisect large boxes
8:           ([x1], [x2]) ← bisect([xc])          Bisect the box
9:           L ← (L, [x1], [x2])                  Enqueue the subboxes
10:       else                                     Don't further process small boxes
11:          X̄ ← X̄ ∪ [xc]
12:       end if
13:    end if
14: end while
15: X̄ ← X̄ ∪ L                                     Add pending boxes to the solution
```

Sensor measurements are affected by noise and may contain outliers due, for instance, to NLOS signal propagation. The set $\mathbb{X}$ of all parameters consistent with the measurements might then be empty, or do not contain the true configuration. A solution to overcome this situation is to define $\mathbb{X}$ as the set of all parameters consistent with at least $m-q$ measurements. This method is the so-called *q-relaxed intersection* [19], denoted $\bigcap^{\{q\}}$ and represented in Figure 4.

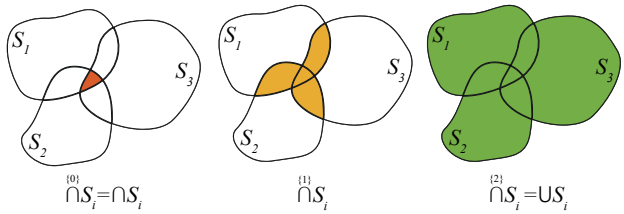

Figure 4: q-relaxed intersection for $q \in \{0, 1, 2\}$

Computing a reliable pose confidence domain, i.e., a box in which the wheelchair is guaranteed to belong, only requires an outer approximation of $\mathbb{X}$. The *Robust Set Inversion via Interval Analysis* (RSIVIA) algorithm [14] computes an outer subpaving of the q-relaxed solution. It is computed the same way as in Algorithm 1, but with a contractor for the q-relaxed intersection as input. The value of q can be estimated at each measurement epoch, using the *Guaranteed Outlier Minimal Number Estimator* (GOMNE) [15, 6]. This algorithm increases the number of relaxed constraints q until a non-empty solution set is found with RSIVIA. Thus, it returns the minimal number of constraints to relax. This section has presented the basic concepts needed to develop our robust interval-based positioning method. The results of Algorithm 1 are presented in Section 5.

4 Interval-Based Reliable State Estimation

In this section, we present our interval-based method to solve the state estimation problem, in the presence of outliers. Only a bounded-error model is assumed. No other assumptions about the distribution and independence of measurement errors are made, contrary to probabilistic methods.

The problem is defined as a CSP, and the constraints are presented in the following subsections. The variables of the problem, and domains we seek to reduce, are the position of the tags in $\mathcal{F}_w$, denoted $\mathbf{x}_{T_i} \in [\mathbf{x}_{T_i}]$, and the wheelchair configuration $\mathbf{p} \in [\mathbf{p}]$. The larger the domains, the higher the uncertainties. Thus, we seek to contract them by removing all the configurations that are not consistent with the constraints.

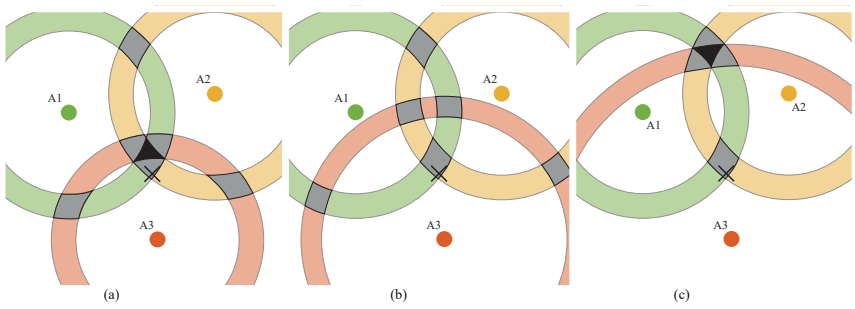

Figure 5: Set-membership localization with three anchors, with one unidentifiable outlier. The solution set is represented in black. The black cross is the actual tag position. The 1-relaxed solution set is represented in gray.

4.1 Constraints over a single epoch

At a given time k or *epoch*, the wheelchair is in a configuration $\mathbf{p}_k = (x_k, y_k, \theta_k)$. Assuming known bounds on range measurement errors, the UWB ranges are represented by a box of interval distances $[\mathbf{r}]_k = ([r_{1,1}]_k, [r_{1,2}]_k, \ldots, [r_{n_A,n_T}]_k)^{\mathbf{T}}$. Considering all these ranges, and the geometry of the problem, a set of constraints can be derived at each epoch k (epoch index k is omitted in the notation). These constraints are presented in this subsection.

UWB constraints in LOS conditions

$\mathcal{L}_{r_{i,j}}$ expresses the distance constraint between the tag T_i and the anchor A_j. It is defined by

$$\mathcal{L}_{r_{i,j}} : \{r_{i,j} = \|\mathbf{x}_{T_i} - \mathbf{x}_{A_j}\|_2\},\ r_{i,j} \in [r_{i,j}],\ i \in \{1 \ldots n_T\},\ j \in \{1 \ldots n_A\}. \tag{3}$$

These constraints are written considering LOS signal propagation for $[r_{i,j}]$ measurement error bounds.

Robustness scheme for the multipath case

The multipath case is handled by the constraint relaxation technique with GOMNE. In the case of an identifiable outlier (i.e., inconsistent with all other measurements), the constraint relaxation strategy can be seen as a measurement rejection scheme. Indeed, in such a case, the non-relaxed solution is empty, and 1-relaxed solution corresponds to the set of all tag positions that are consistent with all measurements except the identifiable outlier.

The case of an unidentifiable outlier is illustrated in Figure 5. In such conditions, the solution set resulting from all constraints is either empty (b), or does not contain the true solution ((a) and (c)), whereas it is the case for the relaxed solution set. The GOMNE algorithm is used to compute the minimal number $q_{\min}$ of constraints

to relax in order not to compute an empty solution set. Thus, a value of $q_{\min} = 0$ will be returned for conditions (a) and (c), and the true solution will not belong to the corresponding solution set. To prevent such a situation, the value computed by GOMNE is then incremented by one to give an additional protection layer against an undetected outlier, such that $q = q_{\min} + 1$.

Wheelchair geometry constraints

The positions of the tags and the wheelchair configuration are linked by geometrical constraints

$$\mathcal{L}_{\mathbf{p},\mathbf{x}_{T_i}} : \left\{ \begin{array}{l} x_{T_i} = x + {}^r x_{T_i} \cos\theta - {}^r y_{T_i} \sin\theta \\ y_{T_i} = y + {}^r x_{T_i} \sin\theta + {}^r y_{T_i} \cos\theta \end{array} \right\}, i \in \{1 \dots n_T\}. \tag{4}$$

The two above constraints are fundamental, since they enable propagating constraints from UWB range measurements to the wheelchair configuration. However, redundant constraints can be added to better contract the variables' domains, thus reducing the uncertainties. Coordinates of the tags, expressed in $\mathcal{F}_r$, are known. The inter-tag distances d_{T_i,T_j} can also be computed. Let ${}^r x_{T_{i,j}} = {}^r x_{T_i} - {}^r x_{T_j}$ and ${}^r y_{T_{i,j}} = {}^r y_{T_i} - {}^r y_{T_j}$ be the difference between the coordinates of i^{th} and j^{th} tag expressed in $\mathcal{F}_r$. This leads to these redundant constraints:

$$\mathcal{L}_{\mathbf{x}_{T_i},\mathbf{x}_{T_j}} : \left\{ \begin{array}{ll} x_{T_i} & = x_{T_j} + {}^r x_{T_{i,j}} . \cos\theta - {}^r y_{T_{i,j}} . \sin\theta \\ y_{T_i} & = y_{T_j} + {}^r x_{T_{i,j}} . \sin\theta + {}^r y_{T_{i,j}} . \cos\theta \\ d_{T_i,T_j} & = \|\mathbf{x}_{T_i} - \mathbf{x}_{T_j}\|_2 \end{array} \right\}, \\ (i,j) \in \{1 \dots n_T\}^2, i < j. \tag{5}$$

Single epoch pose-domain computation

All the constraints related to UWB sensors for a given epoch define a *constraint graph*, presented in Figure 6. We define $\mathcal{L}^k_{\text{UWB}}$ as the composition of (3), (4), and (5) at a given epoch. A contractor is created from $\mathcal{L}^k_{\text{UWB}}$, using the *forward-backward* algorithm [14]. We then set an initial domain for the wheelchair configuration. Finally, we apply GOMNE and the RSIVIA algorithm with the defined contractor, to compute an outer subpaving of all feasible wheelchair poses that are consistent with all measurements except q of them. Notice that, for each epoch k, the computation of the subpaving w.r.t UWB constraints graph is independent from previous epochs, and can be seen as an initial localization problem.

4.2 Pose Estimation from Input Commands

As explained in section 4.1, the wheelchair-configuration domain at epoch k is computed using Algorithm 1 with q-relaxed contractor $\mathcal{L}_{\text{UWB}}$, independently from the previous epoch. To better reduce the estimated pose domain, we use proprioceptive

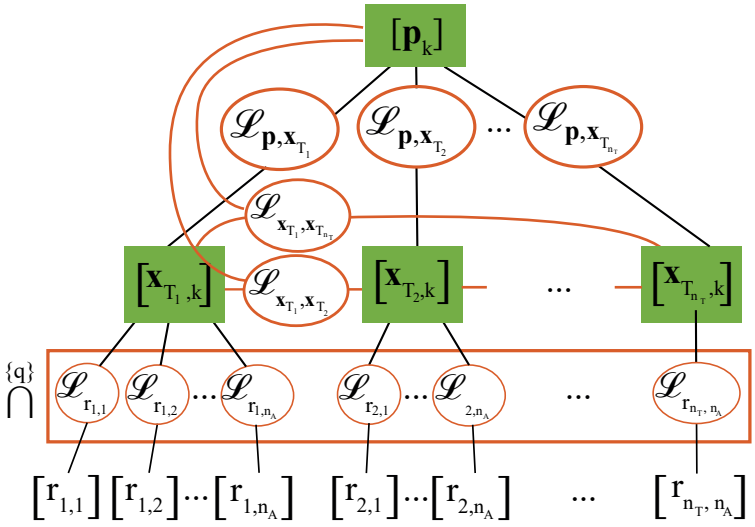

Figure 6: $\mathcal{L}^k_{\text{UWB}}$: UWB-related constraints over a single epoch k . The tag positions are contracted with a robust q-relaxed constraint propagation of the range measurements. Geometrical constraints then contract the wheelchair configuration domains.

information, in the form of linear and angular velocities (v_k, ω_k) directly read from the wheelchair power module.

Discretizing model of (1) using Euler's method, with a sampling period T, the evolution constraints are defined by

$$\mathcal{L}_{\mathbf{p}_{k-1},\mathbf{p}_k} : \left\{ \begin{array}{l} x_{k+1} = x_k + T \cdot v_k \cdot \cos\theta_k \\ y_{k+1} = y_k + T \cdot v_k \cdot \sin\theta_k \\ \theta_{k+1} = \theta_k + T \cdot \omega_k \end{array} \right\}, v_k \in [v_k],\ \omega_k \in [\omega_k]. \tag{6}$$

Integration errors are insignificant w.r.t. uncertainties on the input commands that are handled by our bounded-error model. Evolution constraints are forward-backward propagated in a window containing a horizon of N previous epochs. If $[[\mathbf{p}_{k-N}], ..., [\mathbf{p}_{k-1}], [\mathbf{p}_k]]$ are the pose domains in the horizon at epoch k, then the next epoch horizon is $[[\mathbf{p}_{k-N+1}], ..., [\mathbf{p}_k], [\mathbf{p}_{k+1}]]$. The advantage of such a method is that the evolution constraint propagation related to a wrong configuration domain will only affect domains that share the same horizons. Therefore, N has to be chosen to provide better domain contraction, while not propagating erroneous data over a long period. Evolution constraints graph over one horizon is shown in Figure 7.

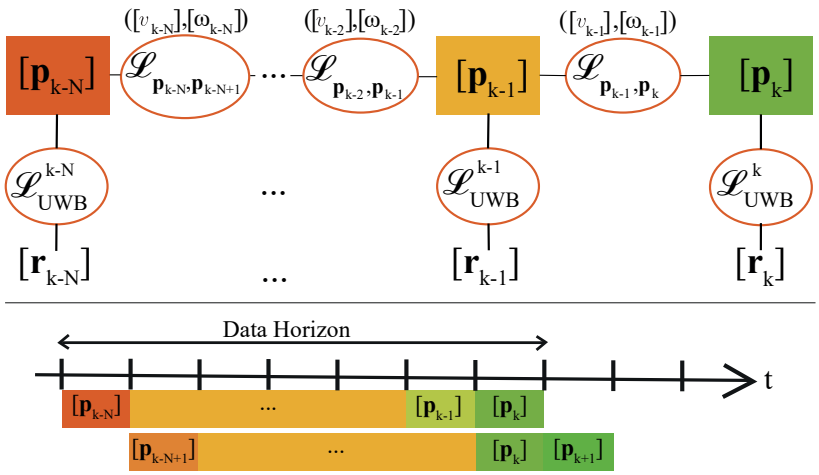

Figure 7: Sliding horizon overview. Robot configuration is computed at each epoch w.r.t. UWB-related constraints. Evolution constraints are then propagated to all variables sharing the same horizon.

5 Experimental Results

5.1 Experimental Setup

To validate our positioning process, we conducted two 4-minute trials using a power wheelchair from Medical Sunrise, which features six wheels: two powered and four caster wheels. Its kinematic is described by the unicycle model of (1). The UWB network was configured by placing 4 UWB anchors in a room and attaching 2 front and 2 rear UWB tags to the wheelchair, as illustrated in Figure 8. UWB range measurements were collected at a frequency of 10 Hz, thus resulting in a total of 4,800 data epochs. Additionally, 8 Qualisys motion capture cameras provide ground truth data for both the wheelchair pose and the positions of the anchors and tags.

During these trials, a user was instructed to navigate the wheelchair using a joystick along a predefined path (see reference trajectory in Figure 12). To mimic real-life activities, the user was tasked to move an object from one table to another located at the opposite end of the room. In the first trial, the user was alone in the wheelchair. In the second trial, a pedestrian walked alongside the wheelchair, occasionally obstructing the line-of-sight (LOS) between some tags and anchors (Figure 9).

We computed the theoretical distances between the anchors and tags and compared them to the measured distances. Figure 10 presents a histogram of the UWB range measurement errors across all trials. The data shows that 85% of the range errors fit a Gaussian distribution with $\sigma = 0.08$ m, corresponding to LOS conditions, while the remaining 15% fit a mixture of Rayleigh distributions, indicative of NLOS conditions.

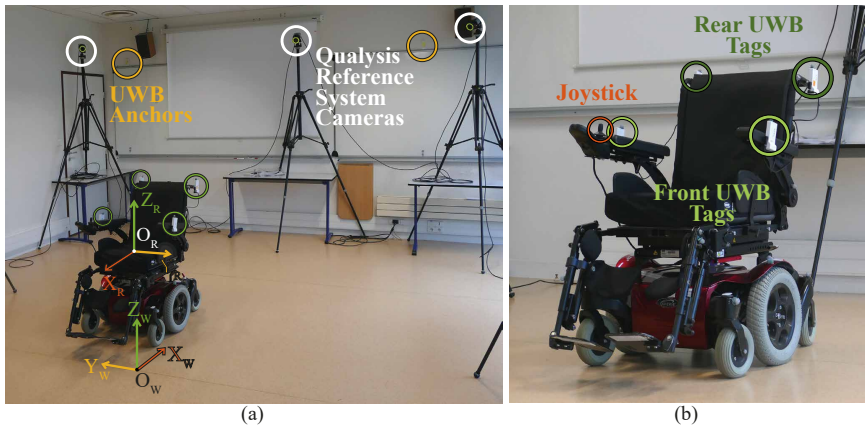

Figure 8: Experimental setup. World frame $\mathcal{F}_w$ and robot frame $\mathcal{F}_r$ are shown in (a).

Figure 9: Experiments without (a) and with (b) a pedestrian. The user had to move the objects from one table to another.

5.2 Pose Domain Computation

The interval-based localization method is tested over both trials. Considering the standard deviation σ estimated in Section 5.1, the UWB range measurement error bounds are set to ± 2.5-σ, i.e., ± 20 cm. With these bounds, 12.82% of the measurements are considered as outliers. UWB anchors' positions are known. Input command error bounds are set to $\pm 0.05 m.s^{-1}$ for linear velocity, and $\pm 0.1 rad.s^{-1}$ for angular velocity. The horizon length is set to $N = 10$, corresponding to 1 s of data. Indeed, a greater N does not provide better domain contraction, thus only increases the risk of propagating an erroneous estimation over a longer time. We assume no prior knowledge of the wheelchair configuration; thus for each epoch, the initial pose domain is set to $[\mathbf{x_0}] = ([-\infty, \infty], [-\infty, \infty], [0, 2\pi])$.

As explained in Section 4.1, all UWB-related constraints, over a single epoch, are

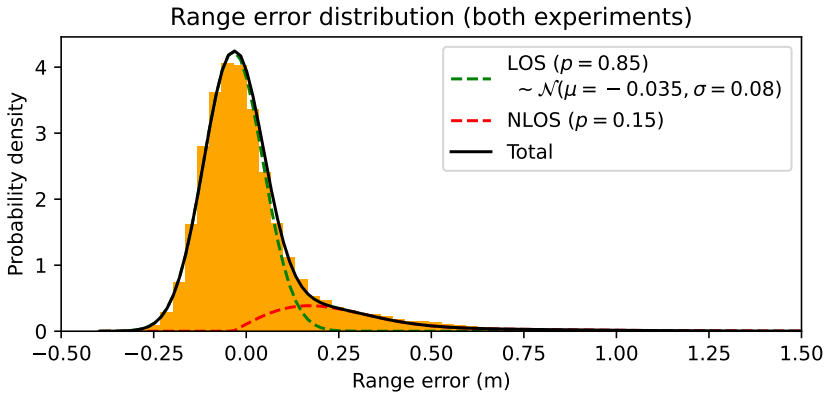

Figure 10: Histogram of the UWB range measurement errors over all trials. 85% of the error distribution is approximated by a Gaussian (green dotted line) in LOS conditions, and 15% by a Rayleigh (red dotted line) in NLOS conditions. The sum of the two distributions fits our range error distribution.

used to create a contractor for the q-relaxed intersection. The q-relaxed contractor is given as input to the RSIVIA algorithm (Algorithm 1), to characterize the set of all feasible poses consistent with the measurements.

At each epoch, 100 ms in total are available to first determine the q value with GOMNE and then compute the pose domain with RSIVIA. A 10 ms budget is allotted to each GOMNE iteration, and all remaining time is then used by RSIVIA to refine the pose domain estimation.

Figure 11 shows outer subpavings (orange boxes) resulting from the RSIVIA algorithm, at epochs corresponding to the minimum (a) and maximum (b) horizontal position error, as well as a disconnected solution set (c). One can observe that these subpavings enclose the ground truth pose (white dots).

Furthermore, the evolution constraints over the horizon enable to significantly reduce our uncertainty domains, as shown by the green boxes in Figure 11. Pose domain contraction using the horizon requires only 3 ms of computation. Thus, the frequency of pose estimation can be increased to provide high-rate predicted poses between two measurement epochs.

At each epoch, as shown in Figure 11, the center of the box $[\mathbf{p}_k]$, denoted $\hat{\mathbf{p}}_k$, is used as an estimation of the unknown wheelchair configuration $\mathbf{p}_k^\star$. Figure 12 shows the estimated trajectory and the ground truth position for the trial with an accompanying pedestrian, with UWB measurements from all four tags.

Our method was tested, for both trials, using data from either all four tags, only the two front tags, or only the two rear tags. Figure 13 shows the cumulative distribution function (CDF) of the horizontal position error (HPE), for each above condition. Slightly higher errors are observed with the presence of a pedestrian

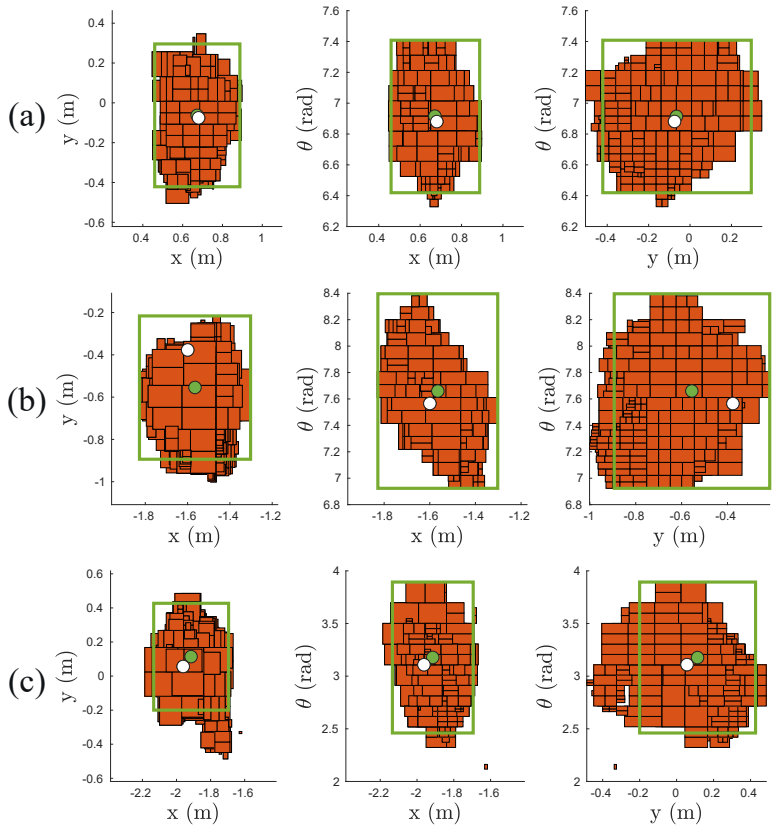

Figure 11: RSIVIA outer subpavings (orange boxes) at $t = 149.4$ s (a), $t = 133.6$ s (b), and $t = 7$ s (c), for the trial with a pedestrian, with four tags. Projections on the x,y plane (*left*), x,θ plane (*middle*) and y, θ plane (*right*). The green boxes represent the box resulting from the contraction of the hull of the orange subpavings, with respect to the evolution constraints. Pose estimate is represented with green dots. Ground truth is represented with white dots.

when using only the two rear tags. This is because the pedestrian was walking next to these particular tags during the experiment. However, when using front or all tags, the CDF are very similar. Thus, the presence of a pedestrian next to the wheelchair has no significant impact on the pose estimation accuracy.

The four-tag solution, with a mean HPE of 6.65 cm (Table 1), is unsurprisingly more accurate than the two-tag solutions. However, the experiments clearly show that using only the two front tags yields better position accuracy (11.44 cm) than the two rear tags (19.46 cm). This is because the position estimate from the rear tags is highly dependent on the orientation estimate, while it is not the case with the two front tags, almost aligned with the robot's y-axis.

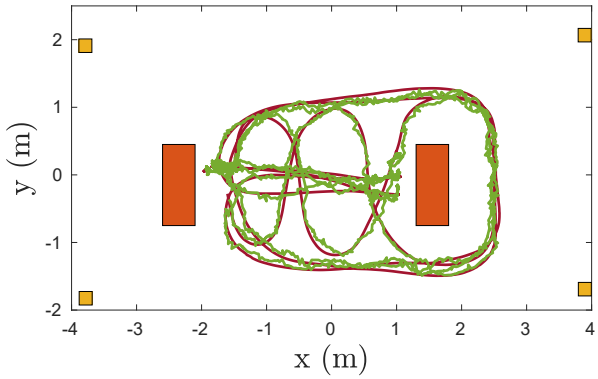

Figure 12: Reference trajectory (red) measured by Qualisys motion capture system, and estimated trajectory (green) with the interval-based localization method, for the trial with a pedestrian, four tags. Tables (orange) and UWB anchors (yellow) are displayed.

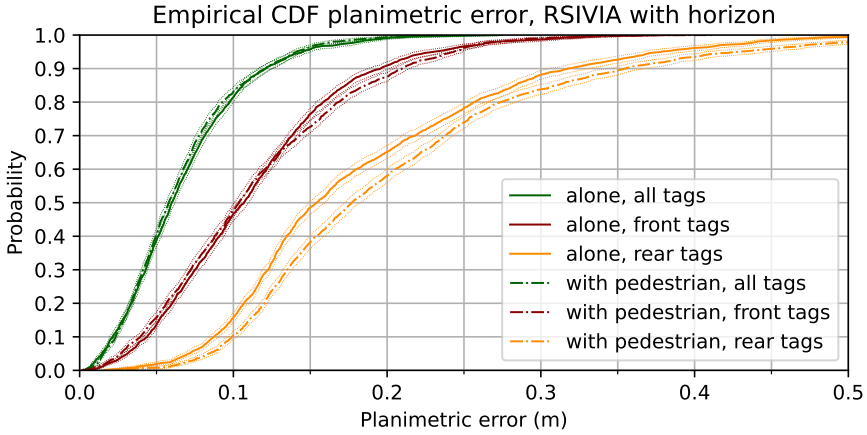

Figure 13: Cumulative Distribution Function of horizontal position error over both trials, with various tag configurations.

To ensure the safety of a task to be performed, each computed pose domain should enclose the true solution. Figure 14 shows the lower and upper bounds of each pose domain, w.r.t. the ground truth, which is at 0. Integrity is obtained if each domain's lower (resp. upper) bound is under (resp. above) the reference line. It can be seen that our method provides confidence domains which are consistent with ground truth, and this is true over the whole dataset. Uncertainties along the x-axis are lower than along the y-axis, due to the geometry of the UWB anchors in the room.

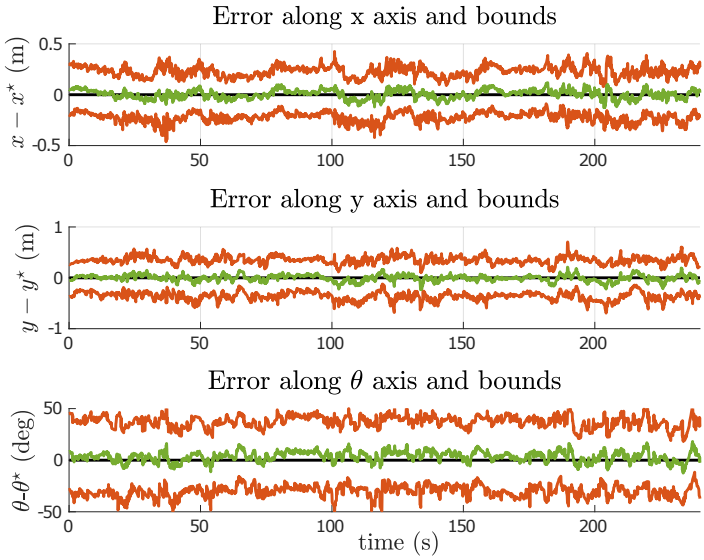

Figure 14: Set-membership position estimation error (green), and confidence lower and upper bounds (orange), for the trial with a pedestrian, with four tags. The reference is at zero (black).

5.3 Comparison with M-Estimator Method

To demonstrate the accuracy of our solution, a comparison with two M-estimators has been carried out, using the same dataset with a horizon of 10 measurement epochs. The first implements the classical Huber loss [12] with 2-σ threshold, and the second a half-Cauchy distribution based loss function, well suited for UWB localization with NLOS [16]. Statistics on the horizontal position error (HPE) and absolute yaw error are given in Table 1. It can be seen that the half-Cauchy M-estimator method is more precise than the classical Huber loss, as shown in [16].

It can be seen that, except when only the two rear tags are used, our interval-based method presents HPE accuracy results close to the half-Cauchy M-estimator method (mean HPE error is 1.76 cm worse). The yaw estimation accuracy is also close (mean absolute yaw error is 0.86° worse) when using all tags, but significantly decreases for both methods when using only two tags. Our method is primarily designed to compute confidence domain in the worst-case scenario, thus is not focused on pose estimate accuracy as it is the case for the M-estimator methods. This explains the better HPE accuracy results for the latter.

We also compared our uncertainty domains with those of the M-estimator method. Results are shown in Table 2. The half-Cauchy M-estimator 3σ bounds on position and angular estimates are significantly smaller than the radius of the computed interval domains (e.g., a mean 3σ radius over x estimate of 4 cm, instead

Table 1: Horizontal position error (HPE) and absolute yaw error $|\tilde{\theta}|$ statistics over both trials, with a horizon of 10 epochs

Method	RSIVIA			M-estimator (Huber)			M-est. (half-Cauchy)		
Tag group	rear	front	all	rear	front	all	rear	front	all.
Mean HPE (cm)	19.46	11.44	**6.65**	11.43	9.03	**5.10**	10.77	8.07	**4.89**
Med. HPE (cm)	16.55	10.50.	**5.90**	10.11	8.67	**4.36**	9.85	7.76	**4.26**
95% HPE (cm)	40.42	23.85	**14.35**	23.88	16.20	**11.86**	21.79	14.65	**11.07**
Max HPE (cm)	70.89	41.17	**27.45**	65.66	28.52	**20.62**	60.64	30.96	**21.14**
Mean $\|\tilde{\theta}\|$ (deg)	13.27	20.12	**5.12**	9.07	8.49	**4.49**	8.77	7.47	**4.26**
Med. $\|\tilde{\theta}\|$ (deg)	10.72	13.92	**4.66**	7.79	7.22	**4.08**	7.64	6.19	**3.84**
95% $\|\tilde{\theta}\|$ (deg)	39.04	58.10	**11.58**	20.79	20.14	**9.93**	19.55	18.32	**9.46**
Max $\|\tilde{\theta}\|$ (deg)	83.18	76.71	**19.56**	45.78	49.18	**22.13**	43.85	57.83	**21.22**

Table 2: Estimation Uncertainty (four tags, both trials) with a horizon of 10: RSIVIA interval domain radius, half-Cauchy (HC) M-estimator with 3σ bounds

Method	RSIVIA: radius			HC M-est.: 3σ			*Consistent HC M-est.:* 3σ		
Domain	x (cm)	y (cm)	θ (deg)	x (cm)	y (cm)	θ (deg)	x (cm)	y (cm)	θ (deg)
min	12.20	21.26	21.48	2.37	3.82	4.17	9.31	15.01	16.37
mean	22.46	35.69	33.43	3.02	4.97	4.95	11.86	19.55	19.46
95%	27.66	43.67	38.49	3.99	5.87	5.27	15.70	23.07	20.70
max	44.05	58.50	51.65	8.13	13.81	16.06	31.95	54.27	63.13

of 22.5 cm with intervals). However, our method provides consistent confidence domains over the whole tested dataset, which is not the case for the half-Cauchy M-estimator method, where the 99% confidence ellipsoid contains the ground truth pose in only 41.7% of the epochs. The latter assumes that measurement errors are independent between two epochs, which is not verified since multipath effects are spatially and therefore temporally correlated, and UWB nodes also have small ranging biases. The 99% confidence ellipsoid needs to be inflated 3.9 times to be consistent with ground truth (i.e. considering a increased measurement error standard deviation of 33 cm). The corresponding uncertainty domains are shown in the last three columns of Table 2. They remain smaller than those provided by our method, but in the same order of magnitude (e.g., a mean 3σ radius over θ estimate of 19.5°, instead of 33.4° with intervals). However, our interval-based method does not need over-tuning to become consistent. It only assumes a bounded-error model, without any independence assumption. Thus, our confidence domains are bigger than those obtained from M-estimator, but no overconfidence is given to the

estimated pose when using realistic measurement error bounds.

The conservative behavior of our method is mostly related to constraint relaxation. Indeed, using the SIVIA algorithm without q-relaxed intersection instead of RSIVIA in our methods results in smaller confidence domains (Figure 15). However, as shown by the blank spaces in Figure 15, the SIVIA method returns an empty solution-set over 86.7% of the dataset, where pose estimation is thus unavailable. It is remarkable that the unavailability of the SIVIA method occurs for large periods of time. This was predictable since multipath are temporally correlated. Our method was designed to provide a high integrity level while ensuring the availability of the localization process. It is then a step toward robust pose estimation for the specific case of UWB for smart wheelchairs.

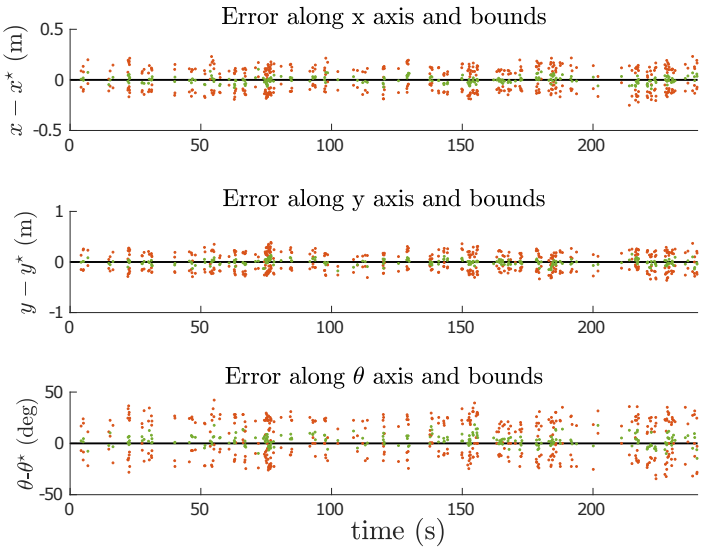

Figure 15: Results of single epoch SIVIA method without constraint relaxation, for the trial with a pedestrian, with four tags. Estimation error in green and bounds in orange (as in Figure 14). The blank spaces correspond to empty solution sets.

6 Conclusion

In this paper, an interval-based localization method for a smart wheelchair has been presented. It provides a real-time robot pose estimate, as well as reliable confidence domains, from bounded-error UWB range measurements and proprioceptive information.

The pose estimation is performed using robust q-relaxed constraint propagation over a horizon of data. The set of the feasible robot poses is computed at each

epoch, using UWB-related constraints. These pose domains are then refined by propagating evolution constraints over the data horizon.

Experiments have been conducted on the smart wheelchair equipped with UWB sensors. Results exhibit consistency of the pose estimation w.r.t. ground truth, despite the large presence of outliers. Close results in terms of accuracy were highlighted when comparing interval-based and M-estimator methods. However, without measurement noise variance inflation, the M-estimator yields inconsistent uncertainty ellipsoids, while our method provides confidence domains that enclose the ground truth 100% of the time over the tested dataset.

The method has been designed to provide worst-case confidence domains, hence its conservative behavior. In order to be exploitable in a fully autonomous navigation and control loop, a trade-off between integrity and confidence domain size could be performed, given a tolerated risk level. Smaller confidence domains could also be computed by developing more efficient contraction methods, and by allocating more time to the GOMNE and RSIVIA algorithms. Also, it seems acceptable to integrate a gyroscope to the smart wheelchair to directly measure the yaw rate with smaller uncertainties, and improve horizon contraction efficiency.

References

[1] Bolting, J. and Fergani, S. Ellipsoidal set membership filtering with reduced conservatism applied to relative localization between aircraft based on GNSS and UWB ranging. In *Proceedings of the 2019 18th European Control Conference*, pages 1810–1815. IEEE, 2019. DOI: 10.23919/ECC.2019.8796256.

[2] Brunacci, V., De Angelis, A., Costante, G., and Carbone, P. Development and analysis of a UWB relative localization system. *IEEE Transactions on Instrumentation and Measurement*, 72:1–13, 2023. DOI: 10.1109/TIM.2023.3305661.

[3] Cazzorla, A., De Angelis, G., Moschitta, A., Dionigi, M., Alimenti, F., and Carbone, P. A 5.6-GHz UWB position measurement system. *IEEE Transactions on Instrumentation and Measurement*, 62(3):675–683, 2013. DOI: 10.1109/TIM.2012.2219139.

[4] Chabert, G. and Jaulin, L. Contractor programming. *Artificial Intelligence*, 173(11):1079–1100, 2009. DOI: 10.1016/j.artint.2009.03.002.

[5] Dardari, D., Conti, A., Ferner, U., Giorgetti, A., and Win, M. Z. Ranging with ultrawide bandwidth signals in multipath environments. *Proceedings of the IEEE*, 97(2):404–426, 2009. DOI: 10.1109/JPROC.2008.2008846.

[6] Desrochers, B., Lacroix, S., and Jaulin, L. Set-membership approach to the kidnapped robot problem. In *Proceedings of the 2015 IEEE/RSJ International Conference on Intelligent Robots and Systems*, pages 3715–3720. IEEE, 2015. DOI: 10.1109/IROS.2015.7353897.

[7] Devigne, L., Narayanan, V. K., Pasteau, F., and Babel, M. Low complex sensor-based shared control for power wheelchair navigation. In *Proceedings of the 2016 IEEE/RSJ International Conference on Intelligent Robots and Systems*, pages 5434–5439. IEEE, 2016. DOI: 10.1109/IROS.2016.7759799.

[8] Drevelle, V. and Bonnifait, P. Localization confidence domains via set inversion on short-term trajectory. *IEEE Transactions on Robotics*, 29(5):1244–1256, 2013. DOI: 10.1109/TRO.2013.2262776.

[9] Finlayson, M. and Van Denend, T. Experiencing the loss of mobility: Perspectives of older adults with MS. *Disability and rehabilitation*, 25(20):1168–1180, 2003. DOI: 10.1080/0963828031000159618O.

[10] Gentner, C., Jost, T., Wang, W., Zhang, S., Dammann, A., and Fiebig, U.-C. Multipath assisted positioning with simultaneous localization and mapping. *IEEE Transactions on Wireless Communications*, 15(9):6104–6117, 2016. DOI: 10.1109/TWC.2016.2578336.

[11] González, J., Blanco, J., Galindo, C., Ortiz-de Galisteo, A., Fernández-Madrigal, J., Moreno, F., and Martínez, J. Mobile robot localization based on Ultra-Wide-Band ranging: A particle filter approach. *Robotics and Autonomous Systems*, 57(5):496–507, 2009. DOI: 10.1016/j.robot.2008.10.022.

[12] Huber, P. J. Robust estimation of a location parameter. *The Annals of Mathematical Statistics*, 35(1):73–101, 1964. DOI: 10.1007/978-1-4612-4380-9_35.

[13] Jaulin, L. Robust set-membership state estimation; application to underwater robotics. *Automatica*, 45(1):202–206, 2009. DOI: 10.1016/j.automatica.2008.06.013.

[14] Jaulin, L., Kieffer, M., Didrit, O., and Walter, É. *Interval Analysis*. Springer, 2001. DOI: 10.1007/978-1-4471-0249-6_2.

[15] Jaulin, L., Kieffer, M., Walter, E., and Meizel, D. Guaranteed robust nonlinear estimation with application to robot localization. *IEEE Transactions on Systems, Man, and Cybernetics, Part C (Applications and Reviews)*, 32(4):374–381, 2002. DOI: 10.1109/TSMCC.2002.806747.

[16] Jiang, F., Caruso, D., Dhekne, A., Qu, Q., Engel, J. J., and Dong, J. Robust indoor localization with ranging-imu fusion. In *Proceedings of the 2024 IEEE International Conference on Robotics and Automation*, pages 11963–11969. IEEE, 2024. DOI: 10.1109/ICRA57147.2024.10611274.

[17] Jiang, H., Wang, W., Shen, Y., Li, X., Ren, X., Mu, B., and Wu, J. Efficient planar pose estimation via UWB measurements. In *Proceedings of the*

2023 IEEE International Conference on Robotics and Automation, pages 1954–1960, London, United Kingdom, 2023. IEEE. DOI: 10.1109/ICRA48891.2023.10161456.

[18] Kenmogne, I.-F., Drevelle, V., and Marchand, E. Interval-based cooperative uavs pose domain characterization from images and ranges. In *Proceedings of the 2018 IEEE/RSJ International Conference on Intelligent Robots and Systems*, pages 6349–6356. IEEE, 2018. DOI: https://doi.org/10.1109/IROS.2018.8593742.

[19] Kieffer, M., Jaulin, L., Walter, E., and Meizel, D. Robust autonomous robot localization using interval analysis. *Reliable Computing*, 6(3):337–362, 2000. DOI: 10.1023/A:1009990700281.

[20] Leaman, J. and La, H. M. A comprehensive review of smart wheelchairs: past, present, and future. *IEEE Transactions on Human-Machine Systems*, 47(4):486–499, 2017. DOI: 10.1109/THMS.2017.2706727.

[21] Ledergerber, A., Hamer, M., and D'Andrea, R. A robot self-localization system using one-way ultra-wideband communication. In *Proceedings of the 2015 IEEE/RSJ International Conference on Intelligent Robots and Systems*, pages 3131–3137, Hamburg, Germany, 2015. IEEE. DOI: 10.1109/IROS.2015.7353810.

[22] Magnago, V., Corbalan, P., Picco, G. P., Palopoli, L., and Fontanelli, D. Robot localization via odometry-assisted ultra-wideband ranging with stochastic guarantees. In *Proceedings of the 2019 IEEE/RSJ International Conference on Intelligent Robots and Systems*, pages 1607–1613, Macau, China, 2019. IEEE. DOI: 10.1109/IROS40897.2019.8968019.

[23] Merlinge, N. Set inversion and box contraction on Lie groups using interval analysis. *Automatica*, 165:111688, 2024. DOI: 10.1016/j.automatica.2024.111688.

[24] Morales, Y., Kallakuri, N., Shinozawa, K., Miyashita, T., and Hagita, N. Human-comfortable navigation for an autonomous robotic wheelchair. In *Proceedings of the 2013 IEEE/RSJ Int. Conf. on Intelligent Robots and Systems*, pages 2737–2743. IEEE, 2013. DOI: 10.1109/IROS.2013.6696743.

[25] Morbidi, F. et al. Assistive robotic technologies for next-generation smart wheelchairs: Codesign and modularity to improve users' quality of life. *IEEE Robotics & Automation Magazine*, 30(1):24–35, 2023. DOI: 10.1109/MRA.2022.3178965.

[26] Mustafa, M., Stancu, A., Guteirrez, S. P., Codres, E. A., and Jaulin, L. Rigid transformation using interval analysis for robot motion estimation. In *Proceedings of the 2015 20th International Conference on Control Systems and Computer Science*, pages 24–31. IEEE, 2015. DOI: 10.1109/CSCS.2015.98.

[27] Pasteau, F., Narayanan, V. K., Babel, M., and Chaumette, F. A visual servoing approach for autonomous corridor following and doorway passing in a wheelchair. *Robotics and Autonomous Systems*, 75:28–40, 2016. DOI: 10.1016/j.robot.2014.10.017.

[28] Rauh, A., Gourret, Y., Lagattu, K., Hummes, B., Jaulin, L., Reuter, J., Wirtensohn, S., and Hoher, P. Experimental validation of ellipsoidal techniques for state estimation in marine applications. *Algorithms*, 15(5):162, 2022. DOI: 10.3390/a15050162.

[29] Rohou, S., Jaulin, L., Mihaylova, L., Le Bars, F., and Veres, S. M. *Reliable Robot Localization: A Constraint-Programming Approach Over Dynamical Systems*. Wiley, 1 edition, 2019. DOI: 10.1002/9781119680970.

[30] Wang, Z. and Lambert, A. A low-cost consistent vehicle localization based on interval constraint propagation. *Journal of Advanced Transportation*, 2018(1):2713729, 2018. DOI: 10.1155/2018/2713729.